Chaos transition in Periodically Driven Oscillators: A Time domain description

Charbel Tannous

Chaos transition in Periodically Driven Oscillators: A Time domain description

C. Tannous

Université de Brest, Lab-STICC, CNRS-UMR 6285, F-29200 Brest, FRANCE

(Dated: March 29, 2023)

We develop a time-domain approach for the transition to Chaos in several periodically driven oscillators by direct integration of first-order ordinary differential equations (ODE) or functional map systems, their discrete-time counterparts. Our theoretical evaluations can be used to make detailed comparisons with experimental measurements in selected oscillating systems starting from the simple mechanical pendulum to electrical circuits: Duffing, Linsay, Testa *et al.* , Colpitts, then to Ikeda opto-electronic setup ... We discuss various types and origins of Chaos in these driven oscillators using bifurcation notions and tying them to some physical properties of their essential components such as Varactor Diodes in RLD (Resistance, Inductance and Diode) circuits or bistable laser excited circular cavities...

PACS numbers: 02.60.Cb, 05.45.Ac, 05.45.Pq, 02.90.+p, 05.40.-a
Keywords: Numerical simulation; solution of equations, Low-dimensional Chaos, Numerical simulations of chaotic systems, Fluctuation phenomena, random processes, noise, and Brownian motion

Contents

I. INTRODUCTION

Oscillators and their transition to Chaos are described starting from the basic mechanical pendulum to tackle continuous time electrical oscillators comprising some non-linear RLD circuits (Resistance, Inductance and a Diode playing the role of a capacitance) as well as the Coplitts oscillator.

Discrete time oscillators described by maps (also called difference equations) are also described such as the logistic, intermittent and the Ikeda maps describing interactions between a laser excited cavity electric field and a non-linear

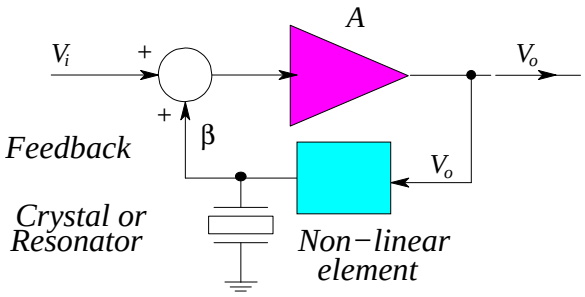

Fig.1: Basic oscillator circuit with a crystal resonator, amplifier and feedback through a non-linear element.

Kerr dielectric.

Conditions for oscillating and routes to Chaos are also both described.

A. Oscillation criteria

An oscillator requires a resonator with amplification A and feedback β (see fig. 1). A resonator could be a crystal or an RLD circuit.

The fundamental condition of oscillation is the Barkhausen criterion shown in fig. 1 and described below.

Oscillatory behavior is induced by an instability (pole in the response when $A\beta = 1$), however we need phase opposition between two key voltages V_β and V_A (Amplifier and feedback voltages) at all times in the circuit.
Sign alternating (phase delay of $\pm\pi$ between V_β and V_A) with equal amplitudes lead to oscillatory behavior and general Barkhausen condition $|A\beta| = 1$.
The simple Barkhausen rule with amplification and linear feedback is not enough to warrant oscillation in presence of noise. We must introduce a non-linear element in the circuit providing a general Barkhausen rule embodying non-linearity.
Thus an oscillator consists of a resonator with three additional components:

1. Amplifier
2. Feedback circuit
3. Non-linear element

Another form of the Barkhausen criterion might be rephrased below with two components A and β as stated previously with a slight modification:

1. Amplifier
2. Feedback circuit containing at least one non-linear element.

B. Mechanical device displaying Chaos

When a pendulum is driven by a periodic force $F\cos(\omega t)$ with ω, the angular resonance frequency having a large amplitude, it undergoes stationary erratic oscillations signaling the onset of Chaos.
Let us apply Euler-Lagrange method to the simple pendulum [1] problem depicted in fig. 2 with θ the generalized coordinate.
The kinetic energy is $T = \frac{1}{2}m(\dot{\boldsymbol{r}})^2$ with velocity $\dot{\boldsymbol{r}} = \ell\dot{\theta}\boldsymbol{e}_\theta$. The derivation with respect to time of some physical quantity such as the geometrical position $\boldsymbol{r}$ is denoted by $\dot{\boldsymbol{r}} = \frac{d\boldsymbol{r}}{dt}$.
Thus $T = \frac{1}{2}m\ell^2(\dot{\theta})^2$ whereas the potential energy is $V = mg\ell(\cos\theta - 1)$ when its origin is chosen at $z = \ell$.
The Lagrangian is $L = T - V$ and Euler-Lagrange equation is:

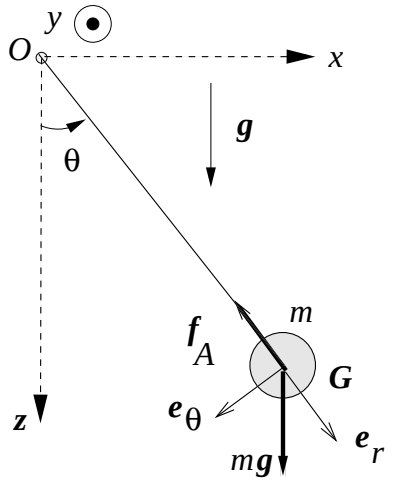

Fig.2: Simple pendulum with attachment force $\boldsymbol{f}_A$ and gravitational force $\boldsymbol{g}$ applied to mass m. Center of mass position G yields $OG = \boldsymbol{r} = \ell \boldsymbol{e}_r$ and its velocity $\dot{\boldsymbol{r}} = \ell\dot{\theta}\boldsymbol{e}_\theta$ where $\boldsymbol{e}_\theta, \boldsymbol{e}_r$ are unit vectors perpendicular to each other.

$$\frac{d}{dt}\left(\frac{\partial L}{\partial \dot{\theta}}\right) - \frac{\partial L}{\partial \theta} = 0, \quad \ddot{\theta} + \frac{g}{\ell}\sin\theta = 0 \tag{1}$$

The second time derivative of θ is denoted by $\ddot{\theta} = \frac{d^2\theta}{dt^2}$.

The above equation of motion can be retrieved with the traditional torque method (see fig. 2) by writing:

$$J\ddot{\theta}\boldsymbol{y} = \boldsymbol{r} \times (\boldsymbol{f}_A + m\boldsymbol{g}) = \boldsymbol{r} \times m\boldsymbol{g} = -mg\ell\sin\theta\boldsymbol{y} \tag{2}$$

where $J = m\ell^2$ is the moment of inertia of the mass m with respect to a massless rod attachment point O and $\boldsymbol{y}$ is a unit vector perpendicular to pendulum plane as shown in fig. 2.

In presence of damping γ opposed to velocity and excitation with a harmonic force $F\cos(\omega t)\boldsymbol{e}_\theta$ where $\omega = \sqrt{m - \gamma^2/4}$ is the angular resonance frequency, the equation of motion is transformed into:

$$J\ddot{\theta} = F\ell\cos(\omega t) - mg\ell\sin(\theta) - \gamma\ell\dot{\theta} \tag{3}$$

The pendulum shows regular oscillations when small F excitation amplitudes are used as displayed in fig. 2.

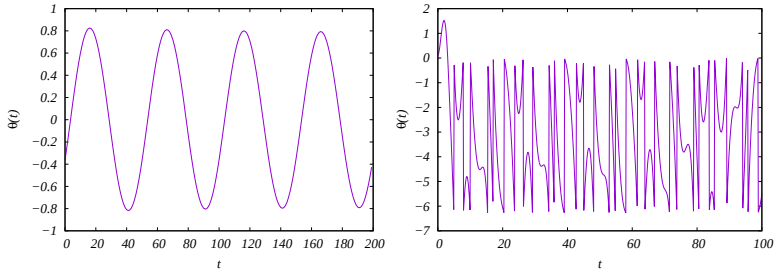

$(F\ell/J) = 0.1$ $\qquad$ $(F\ell/J) = 2.0$

Fig.3: (Left) Pendulum oscillations with a timestep given by $h = \frac{1}{50}(2\pi/\omega)$ where $\omega = \sqrt{m - \gamma^2/4}$. The excitation amplitude is small $(F\ell/J) = 0.1$. (Right) Chaotic pendulum behavior with a large excitation amplitude $(F\ell/J) = 2$.

Mathematically, all non-linear dynamical systems with more than two degrees of freedom, display chaotic behavior whereas discrete-time maps with only a single degree of freedom can display chaotic behavior. The pendulum possess two degrees of freedom: θ and $\dot{\theta}$, thus one expects chaotic behavior for large amplitude excitation as displayed in fig.3.

C. Transition routes to Chaos

Many time-dependent or dynamical systems such as mechanical (pendulum...), electronic circuits, lasers, chemical reactions, periodically stimulated cardiac cells, turbulence in fluids and gases display Chaotic behavior characterized by sensitivity to initial conditions, apparent stationary random behavior with short-term predictability and long-time unpredictability.

Landau was the first to describe in (1944, 1959) the transition to Chaos from the Fluid Mechanics point of view. In the Turbulence chapter of his Fluid Mechanics book [2] he described it as due to a succession of the appearance of different periods until the fluid velocity spectrum looked like white noise.

Landau considered fluid time turbulence as the limit of an infinite sequence of instabilities each of which displaying a new frequency. Later, Newhouse, Ruelle and Takens [3] showed that after only two instabilities at the third step [1], the trajectory becomes attracted to a bounded region of phase space into which trajectories initially close, increase exponentially their mutual distance, making continuously orbit change to reach a chaotic state.
These phase space regions are called strange attractors possessing a self-similar fractal structure embodying geometrical sensitivity to initial conditions, with display of apparent random behavior and implying short-term predictability but long-time unpredictability.

It is believed there are essentially three routes to Chaos [1] based on the notion of bifurcation.
A bifurcation is understood as follows [4]:
Consider an nth-order continuous-time system described by a system of first-order ODE:

$$\frac{dx_i}{dt} = f_i(x_1, x_2...; \alpha), \qquad i = 1...n \tag{4}$$

with a parameter $\alpha \in \mathcal{R}$ and $x_i, f_i, i = 1...n$ are n dimensional variables and functions. As α changes, the limit sets of the system also change. Limit sets are defined by the ensemble of geometrical objects to which the continuous-time system evolve when time $t \to \infty$.
Typically, one expects a small change to produce small quantitative change in a limit set. For instance, slightly varying α could change the position of a limit set in the same fashion, and if the limit set is not an equilibrium point, its shape or size could also change. Moreover it is possible that a small change in α may cause a limit set to undergo a qualitative change. This is called a bifurcation meaning alteration of stability and is similar somehow to a paradigm shift.

Several types of bifurcations are described in the main text and in the Appendix.

The three routes to Chaos are:

1. Pitchfork bifurcation with infinite cascade of period doublings with universal scaling parameters
2. Tangent bifurcation with Intermittent transition to Chaos
3. Hopf bifurcation with three bifurcations leading eventually to a strange attractor with a self-similar fractal structure

Let us detail below each bifurcation case.

1. Pitchfork bifurcation and the Logistic Map

Pitchfork bifurcation was pioneered by Feigenbaum [5] and is observed in driven non-linear oscillators, optical instabilities Rayleigh-Bénard experiments (see Appendix) and Chemical Oscillations.

Maps are the discrete time version of continuous time systems described by arrays of first-order ODE's much like digital filters when compared to their analog counterparts. Maps are also called difference equations.

Let us consider the following recursion $x_{n+1} = ax_n(1 - x_n)$. It is a one-dimensional map with a single degree of freedom x_n and appeared for the first time in 1845 by P. F. Verhulst [1] to simulate the growth of some species population on some bounded piece of land.

The number of species x_{n+1} in year $n+1$ is proportional to the previous year number x_n and to the surface of land reduced proportionally to x_n, implying $x_{n+1} = ax_n(1-x_n)$ where the parameter a depends on the species reproduction rate, available resources in the piece of land and other environmental parameters.
Another example is a bank savings account with a self-limiting rate of interest [6]. Consider a deposit amount of z_0 growing with an interest rate r such that $z_{n+1} = (1+r)z_n$ where n is a discrete time index.
This relation when iterated in time with index n leads to $z_{n+1} = (1+r)^{n+1}z_0$ leading to unlimited capital gain. If a banker wants to limit gain, one possibility is to reduce the rate of interest proportionally to z_n, substituting $r_0(1-\frac{z_n}{z_{max}})$ to r. Consequently the capital develops according to $z_{n+1} = (1+r_0(1-\frac{z_n}{z_{max}}))z_n$ which is equivalent to the logistic map with: $a = 1+r_0, x_n = \frac{r_0}{(1+r_0)}\frac{z_n}{z_{max}}$.

The main property of the logistic map is its limit value called a fixed point when time or index $n \to \infty$. The fixed point x^* is such that when $n \to \infty$ $x_{n+1} \to x^*$ and $x_n \to x^*$ yielding from $x^* = ax^*(1-x^*)$ $x^* = 1 - 1/a$ if we assume that $x^* \neq 0$.

What is also peculiar about the logistic map is that it possesses interesting behavior when a is changed.

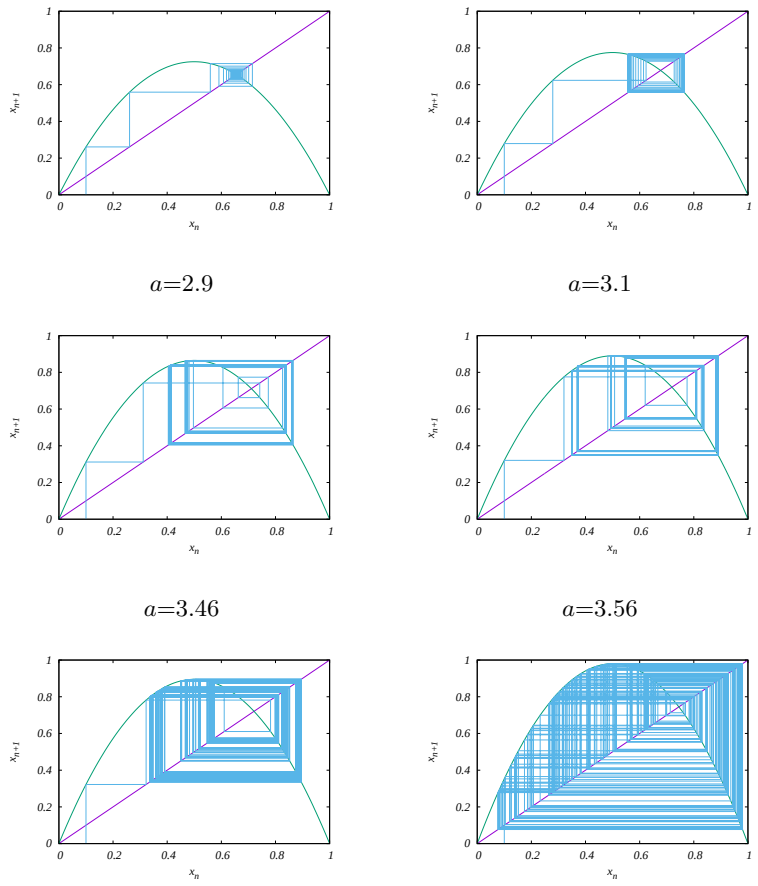

Fig.4: Fixed point, limit cycle or single period, period doubling, quadrupling, octupling and finally chaotic behavior of the logistic map when a= 2.9, 3.1, 3.46, 3.56, 3.58 and 3.92 respectively. All iterations start from 0.1 and the number of periods is indicated by the number of rectangular dense trajectories with a darker color.

Remark on Chaos and non-linear systems
Actually it is surprising to get from a non-linear system, period doubling, period quadrupling... since a non-linear system is supposed to transform a frequency into its higher harmonics.
If we have, for instance, a signal of the form $x(t) = \sin\omega t$ and take its square $x^2(t)$ we end up with 2ω since $\cos 2\omega t = 1 - 2\sin^2\omega t = 1 - x^2(t)$, whereas period doubling leads to $\omega/2$, a sub-harmonic and same with period

quadrupling that leads to $\omega/4$ another sub-harmonic.

Generation of harmonics and subharmonics of a given frequency is important in Music synthesis, signal processing and Telecommunication in areas such as modulation, demodulation, multiplexing, demultiplexing [7]...

2. Tangent bifurcation and Intermittency

Tangent bifurcation was pioneered by Pomeau and Manneville [8] and is observed in Lasers, Chemical reactions, Josephson junctions and Rayleigh-Bénard experiments (see Appendix).

Intermittency [9] arises commonly in systems where the transition from periodic to chaotic behavior takes place by a saddle-node bifurcation (see Appendix). Intermittency is almost a periodic motion interrupted by irregular bursts. Time interval between bursts is a random variable, despite the fact the underlying system is deterministic.

As an example, let us consider a dynamical system described by a variable $x(t)$ a function of time t, that varies almost periodically smoothly for some time interval followed by anarchic bursts as for instance, the Farey map:

$$x_{n+1} = f(x_n), \quad f(x) = \begin{cases} \frac{x}{(1-x)} & x \in [0, 1/2] \\ \frac{(1-x)}{x} & x \in (1/2, 1] \end{cases} \tag{5}$$

It displays intermittency with episodes of smooth or laminar motion and bursty or random behavior as in fig. 5.

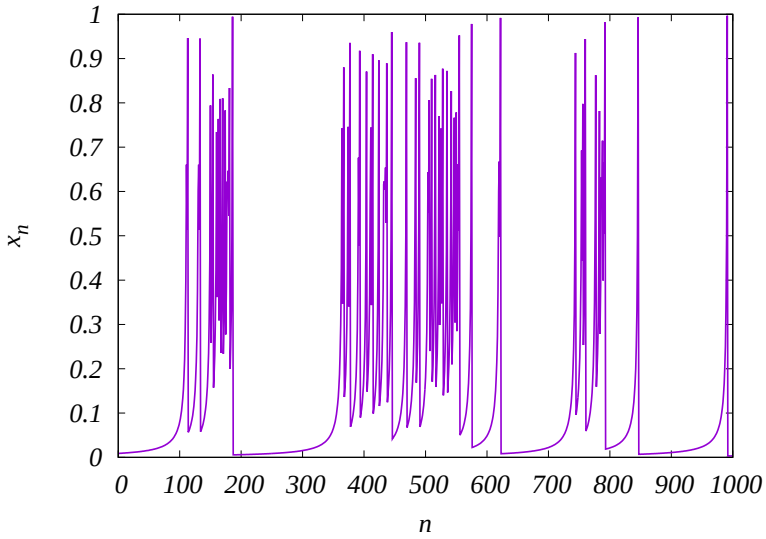

Fig.5: Farey map series displaying alternating smooth and bursty behavior. The starting point of the series $x_0 = 0.0088878$ illustrates the sensitivity to initial conditions well known in chaotic systems, implying that any minute change in the value of x_0 results in a totally different series.

According to Pomeau and Manneville [8], three types of intermittency described by maps are possible depending on the action of some control parameter ϵ. Other types exist such as On-Off and Spatio-Temporal [1].

Type I intermittency originates from saddle-node bifurcation and can be explained in a straightforward way with maps. Let us consider the following 1D map having a bifurcation point $x = 0$:

$$x_{n+1} = \epsilon + x_n + a x_n^2 \tag{6}$$

The saddle point occurs through a sign change of parameter ϵ. When $\epsilon > 0$ there is no fixed point x^* since there is no real solution to $x^* = \epsilon + x^* + a[x^*]^2$ whereas when $\epsilon < 0$ the solution is $x^* = \sqrt{-\epsilon/a}$.
For positive but small ϵ, a narrow tunnel exists between the map function $\epsilon + x_n + a x_n^2$ and the main diagonal $x_{n+1} = x_n$. There are episodes of stable behavior (laminar phase) followed by bursts (chaotic phase) and the

mean length of the laminar phase scales as $1/\sqrt{\epsilon}$. When ϵ decreases, a saddle-node bifurcation occurs with a stable fixed-point attractor at $-\sqrt{-\epsilon}$ and an unstable fixed point at $\sqrt{-\epsilon}$.

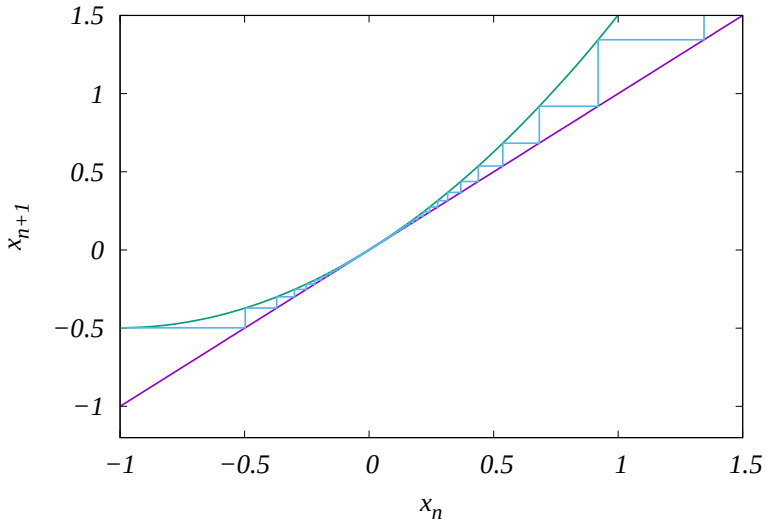

Fig.6: Map $x_{n+1} = \epsilon + x_n + +ax_n^2$ behavior as a function of iterations with $a = 0.5$ and $\epsilon = 0.025$ with the starting point $x_0 = -1$. Remarkably, despite the fact, the iterates trajectory might be stopped by the tangency of the main diagonal to the parabola $\epsilon + x_n + ax_n^2$ around $x = 0$, it proceeds by squeezing itself through the tunnel and emerges afterwards much like a quantum mechanical wave-function traveling across a barrier.

3. Hopf bifurcation and Opto-electronics

Hopf bifurcation [1] was pioneered by Ruelle-Takens-Newhouse [3] and is observed in non-linear conductors, Taylor and Rayleigh-Bénard experiments (see Appendix) as well as in optically bistable systems.
It occurs when a complex-conjugate pair of eigenvalues of an equilibrium point pass through the imaginary axis, thereby creating a limit cycle or closed orbit (see Appendix).

Numerous non-linear optic or opto-electronic devices have been suggested as models that can exhibit chaotic behaviour. There are at least three possibilities:

1. Chaos might me generated with a single non-linear discrete (in time) recursion but needs at least two first-order differential equations that are continuous in time. The dynamics of class-B single-mode lasers is ruled by two first-order differential equations. Waveguide lasers are generally used for single longitudinal or transverse-mode operation; by modifying slightly the resonator configuration to achieve multi-transverse mode emission Chaos becomes observable. It is due in this case to the non-linear interaction of two transverse modes when the cavity length is driven slightly away from the stable operation.
2. Increasing the non-linearity giving birth to Solitons beyond a certain limit above which Soliton propagation is no longer sustainable. Practically, this is done through pumping of the non linear medium with a train of pulses AU_{sol} with U_{sol} a soliton whose amplitude A is increased from one run to the next until propagation failure.
3. The non-linearity might be tuned between radiation emitted or scattered by the medium (Optical fiber for instance) and the pump, when its level exceeds some threshold.

A first route to Chaos is the interaction between the electric field complex envelope and a non-linear medium in a bistable circular cavity called the Ikeda model [10].

Ikeda [10] viewed the non-linear absorbing medium as an ensemble of two-level atoms placed in a ring cavity (see fig. 7) and subjected to a constant light excitation. When the total length of the cavity is large enough, the optical system undergoes a time-delayed feedback destabilizing its steady state output. Ikeda derived from a plane-wave model a set of Differential-Delay equations (DDE) on the basis of the following assumptions:

1. Saturable absorption is ignored.
2. The response time of the non-linear medium is much faster than the cavity round trip time Δt.
3. The non-linear interaction between the medium and the Electric field is of the non-linear Kerr type (The refractive index of the non-linear medium varies with the square of the Electric field amplitude).

In order to simplify Ikeda plane-wave model, Moloney *et al.* [11] derived from it a complex non-linear recursion map (i^2=-1):

$$E_{n+1}(t,x) = a + RE_n(t,x)\exp i(\phi - p/(1+|E_n(t,x)|^2)) \tag{7}$$

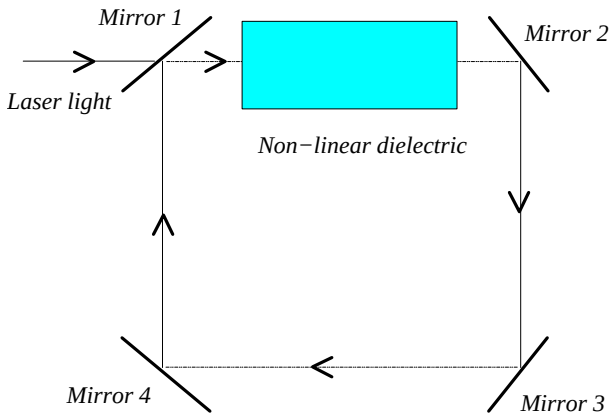

Fig.7: Four mirror ring cavity resonator interacting with a Kerr non-linear dielectric medium.

$E_n(t,x)$ is the Electric Field Complex Envelope at the n-th pass in the cavity (If Δt is the trip time round the cavity, we define instant t as $t = n\Delta t$) at position x along the line crossing the cavity between Mirrors 1 and 2. a is a dimensionless input amplitude, R is the reflectivity of the mirrors, ϕ is the laser empty-cavity detuning factor and p is proportional to linear absorption.

The bifurcation analysis is based on the behavior of a complex map function recursion [10] of the form $z_{n+1} = g(z_n)$ where $z_n = E_n(t,x)$ is the electric field complex envelope and $g(z)$ a complex function given by: $g(z) = a + Rz\exp i(\phi - p/(1+|z|^2))$.

The map recursion stability can be analyzed exactly as a function of parameters a, R, ϕ, p like any set of real maps (see Appendix and Ref. [10]) by transforming the complex map into a 2D real map with $z = x + iy$ we get:

$$\begin{aligned} x_{n+1} &= a + R[x_n\cos A_n - y_n \sin A_n] \\ y_{n+1} &= R[x_n \sin A_n + y_n \cos A_n] \end{aligned} \tag{8}$$

with $A_n = \phi - p/(1 + x_n^2 + y_n^2)$.

The fixed point is given by $z^* = g(z^*)$ yielding the system:

$$\begin{aligned} |g(z^*) - a| &= R|g(z^*)| \\ \cos\left(\frac{p}{1+|g(z^*)|^2} - \phi\right) &= \frac{1}{2R}\left(1 + R^2 - \frac{a^2}{|g(z^*)|^2}\right) \end{aligned} \tag{9}$$

At $z = z^*$, the eigenvalues λ_1, λ_2 of the Jacobian are given by:

$$\begin{aligned} \lambda_1 = R(-D - \sqrt{D^2-1}), \quad \lambda_2 = R(-D + \sqrt{D^2-1}) \\ D = -\frac{p|g(z^*)|^2}{(1+|g(z^*)|)^2}\sin\left(\frac{p}{1+|g(z^*)|^2} - \phi\right) - \cos\left(\frac{p}{1+|g(z^*)|^2} - \phi\right) \end{aligned} \tag{10}$$

From the 2D real map, we get a Jacobian determinant equal to $det[J] = R^2 < 1$, since the reflectivity $R < 1$ and consequently $\lambda_1\lambda_2 < 1$.

Bifurcation requires that an eigenvalue cross the unit circle given by $|\lambda| = 1$.
Thus we have three possibilities [10]:

1. Saddle-node bifurcation: $\lambda_1 = 1$ and the other $\lambda_2 = R^2$, since the Jacobian determinant is $det[J] = \lambda_1\lambda_2 = R^2$.
2. Period-doubling bifurcation: $\lambda_1 = -1$ and $\lambda_2 = -R^2$.
3. Hopf bifurcation: The eigenvalues form a complex-conjugate pair and have to cross the unit circle $|\lambda| = 1$. However, they cannot since $R < 1$ violates the unit circle radius condition.

The bifurcation scenario was found by Moloney [11] who showed that the Ikeda map has two distinct period doubling routes to Chaos and that some periodic cycles, can suddenly occur through a tangent bifurcation as in intermittency to undergo afterwards a period doubling cascade resulting into a strange attractor depicted in Fig. 8.

This scenario is indeed the most frequently favored in ring cavity resonators. Nevertheless when feedback delay in bistable ring cavity resonators becomes arbitrary and we move away from the assumptions previously stated in section I.C.3, Hopf bifurcation regains interest (see for example Ref. [12]).
The second route is a CO_2 waveguide laser using a non standard configuration of the resonator in order to obtain multi-transverse mode operation. Starting from a mirror setup where two modes have a stable coexistence, tiny variations of the cavity length drive the system in the chaotic regime by increasing competition between the transverse modes.

The third Chaos route in Opto-electronics is to exploit our knowledge of Solitons through the use of the generalised (with exchanged space x and time t variables) Non-Linear Schrödinger equation (NLSE) containing a controllable non-linearity function $E(t,x)S(|E(t,x)|^2)$:

$$i\frac{\partial E(t,x)}{\partial x} + \frac{1}{2}\frac{\partial^2 E(t,x)}{\partial t^2} + E(t,x)S(|E(t,x)|^2) = 0 \tag{11}$$

Note that in the standard Schrödinger equation the imaginary term is related to a first-order time derivative whereas in the generalised NLSE, it involves rather a first-order spatial derivative.

The control function is a linear function of $|E(t,x)|^2$ in the ordinary non-linear Kerr case (Medium refractive index varies with the square of the Electric field amplitude). Here it is a smooth function that starts linearly then varies smoothly to saturation as a function of $|E(t,x)|^2$. When the non-linear medium described by the NLSE is pumped with a train of soliton pulses AU_{sol}, the recursion equation for the Electric field complex envelope E_n becomes:

$$E_n(t, x = 0) = AU_{sol}(t, x = 0) + BE_n(t, x = L) \tag{12}$$

where L is the cavity length, n is a pass through the cavity and B is a real number representing mirror losses impacting the cavity output $E_n(t, x = L)$.
After each pass through the cavity a soliton pump pulse is added. The recursion eq. 12 becomes chaotic when the pumping amplitude A is increased beyond a cutoff value. The final scenario is Stimulated Brillouin Scattering (SBS), an important scattering phenomenon in Optical Fibers. It is due to a peculiar type of distributed optical feedback in the fiber and give rise to a positive shift in the input light frequency (Stokes emission phenomenon).

A single-mode fiber can be used to generate SBS above given threshold pump conditions. The non-linear interaction between the pump and the Stokes emission can be tuned in order to give rise to Chaos. The dynamic instability in the fiber is strong and the light intensity (in forward and back-scattering directions) undergoes large fluctuations with modulating depths approaching 100%.

When Chaos is encountered through detection or direct generation (whether high level of pumping or some other large amplitude signal are used) we ought to coerce it into smoother behavior. This is extremely useful in repeater-less long distance communications where the signal to noise ratio should be increased while, simultaneously a smooth behaviour of the signal is required. The control of a chaotic signal is based on the following observation.

Chaos arises from the existence of many unstable periodic orbits that are dense on a strange attractor.

In other words, Chaos arises from the impossibility of the system to settle into a well defined smooth periodic state (i.e. a single characteristic period) for some long enough interval of time. Instead, the system starts in a given state and switches into another one after a small time interval because of the instability. The high density of vicinal periodic states makes the transition easy from one state to another neighboring one.

In order to control the time dependence of the system and force it into a given state with a specific period one needs to probe the local dynamics and estimate from it the local sensitivity of the dynamics with respect to some accessible parameter.

That procedure can be achieved with the algorithm developed by Ott, Grebogi and Yorke [13] and for an illustration of the control method, we extend Ikeda recursion eq. 7, to obtain:

$$E_{n+1}(t,x) = a_n + RE_n(t,x)\exp i(\phi - p/(1+|E_n(t,x)|^2)) \tag{13}$$

where $a_n \in \mathcal{R}$ plays the role of a control parameter. In fact, a_n represents the amplitude of the light pulse penetrating the cavity at time index n. When $a_n = 1$, $\forall n$, the system settles into the chaotic state and the time variation of $E_n(t,x)$ inside the cavity is governed by the map $g(z) = a + Rz\exp i(\phi - p/(1+|z|^2))$ with $a = 1, R = 0.9, \phi = 0.4, p = 6.0$ leading to the Attractor of Fig. 8.

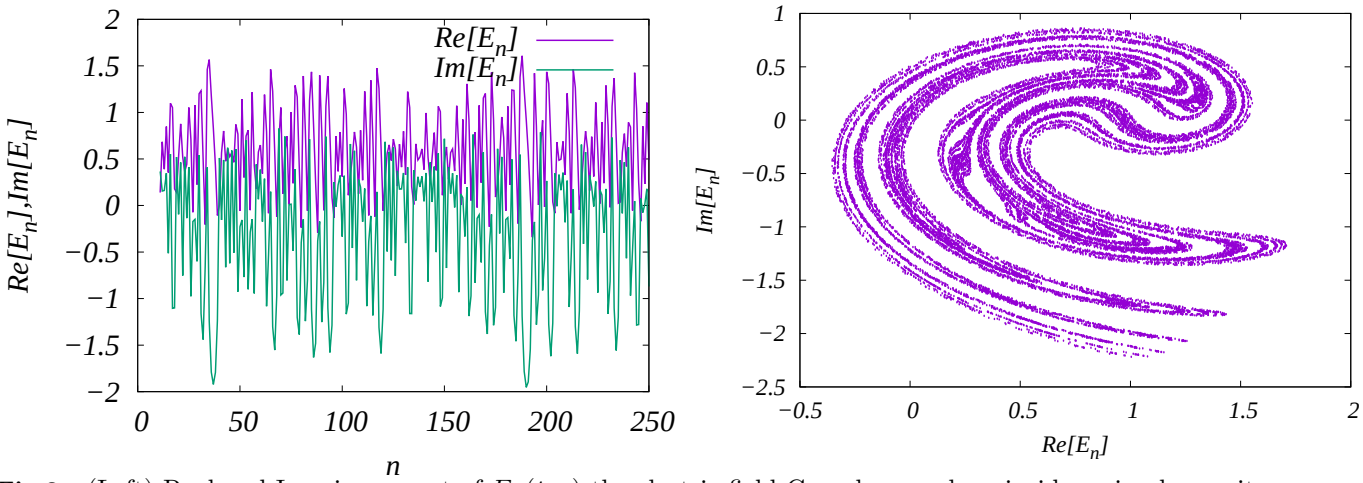

Fig.8: (Left) Real and Imaginary part of $E_n(t,x)$ the electric field Complex envelope inside a circular cavity versus time. (Right) Attractor revealing its fractal self-similar nature with correlation dimension $\nu = 2.6$.

II. DRIVEN NON-LINEAR RLD OSCILLATOR

In this section, we describe first, the non-linear RLD circuit described by Linsay [14] and its critique regarding the origin of Chaos in that circuit.

A periodically driven non-linear RLD circuit is represented by the second-order ODE (Ordinary Differential Equation):

$$L\ddot{Q} + R\dot{Q} + f(Q) = V_0\cos(\omega t) \tag{14}$$

where Q is the time t dependent charge and $f(Q)$ is a non-linear function of Q, V_0 the excitation voltage amplitude and ω the excitation angular frequency. In a simple RLD circuit $f(Q) = Q/C$ where C is a simple capacitance.

A. Duffing oscillator

A general non-linear RLD circuit can be obtained by substituting the circuit capacitance with a reverse biased diode yielding a charge dependent junction capacitance $C(Q)$ resulting into a voltage $V_c(Q) = f(Q) = Q/C(Q)$.

The Duffing [15] oscillator is a particular case embodying a cubic non-linearity $f(Q) = aQ + bQ^3$ where a, b are constants.

$$\begin{aligned} \frac{dQ}{dt} &= I \\ L\frac{dI}{dt} &= -aQ - bQ^3 - RI + V_0\cos(\omega t) \end{aligned} \tag{15}$$

All parameters are normalized for ease of comparison between the Oscillatory and chaotic regimes.

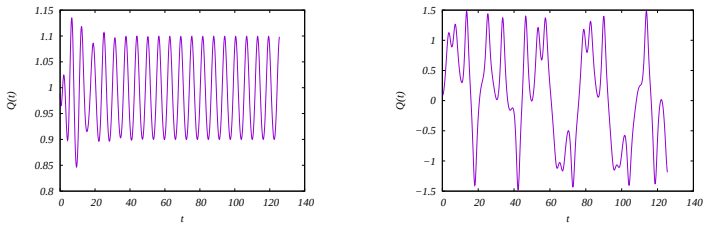

$V_0 = 0.1$ $V_0 = 0.3$

Fig.9: (Left) The Duffing system is driven to oscillation with parameters $a = -1, b = 1$ and $L = 1, R = 0.22, V_0 = 0.1, \omega = 1$. The charge $Q(t)$ oscillates in a very regular fashion after a short transient behavior. (Right) When the excitation amplitude is increased to $V_0 = 0.3$ the charge response $Q(t)$ becomes chaotic.

B. Linsay RLD oscillator

Linsay [14] claimed the time-dependent solution of the ODE 14 is easily obtained through the transformation into a system of two differential equations depending on I, Q variables:

$$\begin{aligned} \frac{dQ}{dt} &= I \\ L\frac{dI}{dt} &= V_0\sin(\omega t) - RI - V_c(Q) \end{aligned} \tag{16}$$

This system is in fact severely ill-conditioned [16] and a better way to tackle it, is to consider instead the variables V_c, I by evaluating the time derivative of V_c. The mathematical difficulty originates from the non-trivial relationship between Q and V_c, since: $Q = C(V_c)V_c$ where $C(V_c) = \frac{C_0}{(1+V_c/\phi)^\gamma}$. C_0 is the zero-bias junction capacitance whereas ϕ and γ are intrinsic voltage scale and exponent proper to the diode.

For instance, the varactor diode 1N5470A used by Linsay [14] and fabricated by Teledyne Crystalonics has the characteristics: C_0= 81.8 pF, ϕ= 0.6 V and γ=0.44.

The excitation drive has angular frequency $\omega = 2\pi f_0$ where f_0 is 1.78 MHz, the resonance frequency of the RLD circuit with R= 180 Ω and L=100 μH, given by:

$$f_0 = \frac{1}{2\pi\sqrt{LC_0 - R^2/4L^2}} \tag{17}$$

Nevertheless, after performing the algebra we get the V_c, I system:

$$\begin{aligned} C_0 \frac{dV_c}{dt} &= I(1 + V_c/\phi)^{(\gamma+1)} \\ L \frac{dI}{dt} &= V_0 \sin(\omega t) - RI - V_c \end{aligned} \tag{18}$$

This system is no longer ill-conditioned and can be integrated by a fourth order Runge-Kutta method [16]. When the drive amplitude V_0=1V, the results are given below in fig. 10:

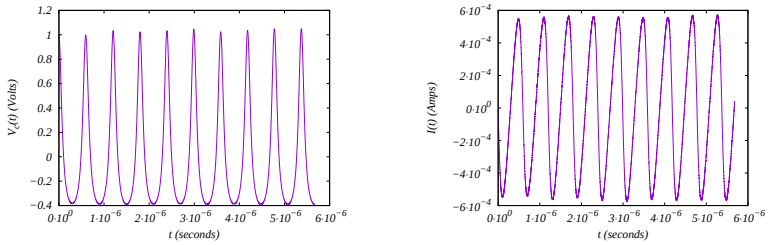

Fig.10: Oscillatory behavior of the variables $V_c(t), I(t)$ when the drive amplitude is relatively small V_0=1 V.

Increasing the amplitude to 3V ,5V and finally 7V yields period doubling, tripling and quintupling versus time as displayed below, in fig. 11:

C. Testa *et al.* RLD oscillator

Testa *et al.* [17] while testing Linsay results, opted for a lower resonance frequency ($\sim$ 90 kHz) and a different type of diode in the RLD circuit.
The varactor diode (type 1N953 supplied by TRW Company), has the junction capacitance characteristics: C_0= 300 pF, ϕ= 0.6 V and γ=0.5.

The RLD circuit is driven by the source $V_0 \sin(\omega t)$ where $\omega = 2\pi f_0$ with f_0 the resonance frequency of the RLD circuit. f_0 is 93 kHz from the RLD circuit characteristic elements given by C_0= 300 pF, R= 28 Ω and L=100 mH.
The RLD circuit becomes a driven anharmonic oscillator exhibiting period doubling, period tripling and quintupling and chaotic behavior.

D. Chaos and varactor diode switching properties

Hunt *et al.* [18] disagreed with the above works by Linsay [14] and Testa *et al.* [17] on the non-linear RLD circuit since both groups attributed period doubling and Chaos to the non-linearity introduced by the voltage-dependent capacitance of the varactor diodes 1N5470A and 1N953 respectively.
In fact, Linsay [14] redid Chaos measurements, replacing the 1N5470A varactor with an 80 pF capacitor in parallel with a 1N4154 diode possessing the same resonance frequency f_0 =1.78 MHz. Nonetheless, the 1N4154 diode setup did not show up bifurcation leading him to assert that the non-linear junction capacitance was indeed the Chaos trigger.

Hunt *et al.* [18] pointed out that another property of those particular 1N5470A and 1N953 diodes was responsible for this peculiar behavior: both have large reverse recovery time in the 100-200 ns range. This was even confirmed by the fact 1N4154 diode having a very short reverse recovery time in the 2-4 ns range did not display Chaos.

Reverse recovery occurs when a forward conducting diode is quickly switched off [19], and the stored charges develop a transient reverse current flow at high reverse voltage.

Ordinary diodes have a reverse recovery time [19] due to charge storage effects, after forward conduction, before they become non-conducting. Typical reverse recovery times are in the 150-200 ns range such as varactor diodes 1N5470A and 1N953 whereas fast recovery diodes with times in the 20-30 ns or even 2-3 ns range are used extensively

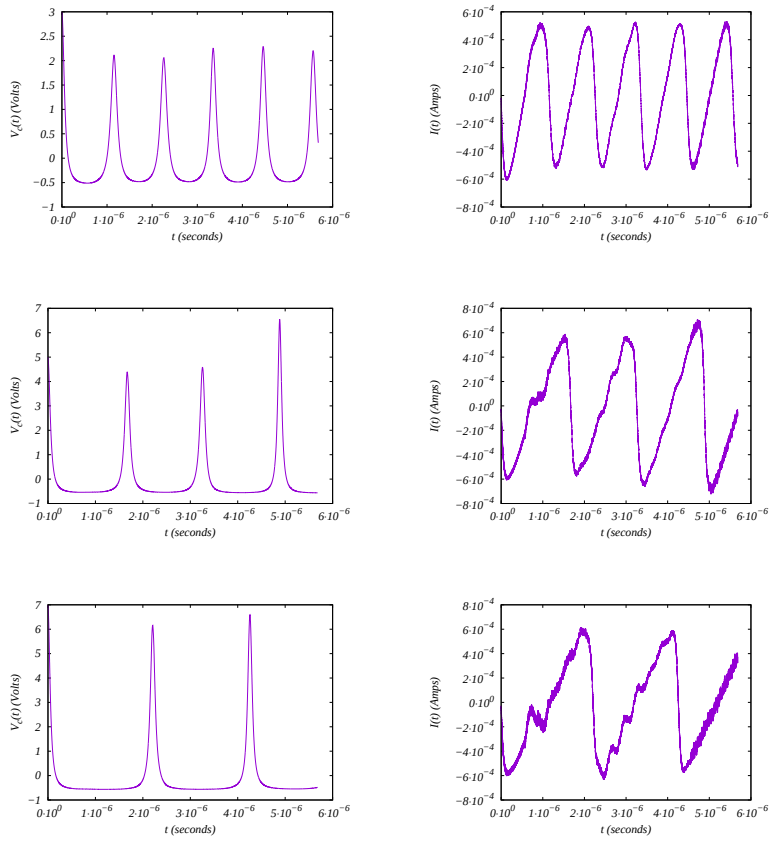

Fig.11: Period doubling, tripling and quintupling behavior of the variables $V_c(t), I(t)$ when the drive amplitude V_0= 3V ,5V and 7V respectively. It is remarkable to observe a smooth variation of the voltage $V_c(t)$ and a noisy $I(t)$ containing different periods of oscillation.

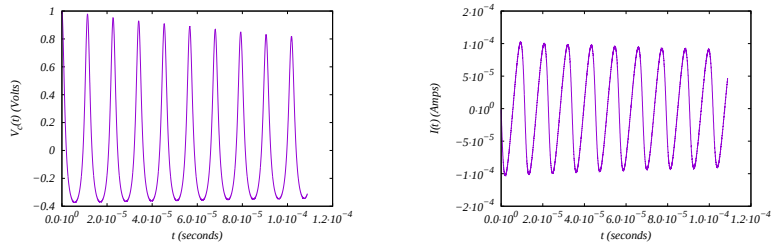

Fig.12: Oscillatory behavior of the variables V_c, I with time when the drive amplitude V_0=1 V.

in high-speed switching particularly in power systems. This is why a diode can be used as a fast soft-recovery rectifier because fast implies it turns off quickly ($<$ 30 ns), and soft means that this operation is not abrupt but somehow very smooth in order to avoid producing large inductive spikes [19], when current transits to non-conduction state (recall $V = LdI/dt$).

On the other hand, Schottky diodes do not have stored charge [19] and therefore no reverse recovery delay. Schottky clamping prevents transistor saturation, which otherwise causes a turn-off delay.

Hunt *et al.* [18] argued that both a finite forward bias voltage and a finite reverse recovery time are required for the particular diode resonator to exhibit chaotic behavior. Moreover they neglected the capacitance variation of the

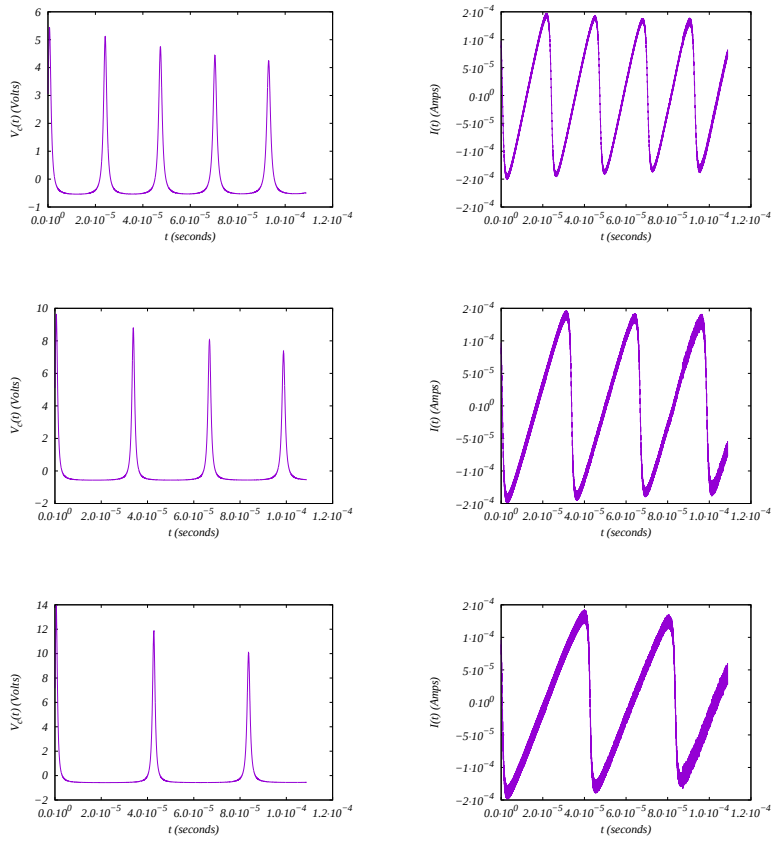

Fig.13: Period doubling, tripling and quintupling behavior of the variables V_c, I with time when the drive amplitude V_0= 3V ,5V and 7V respectively. As in the Linsay case, we observe a smooth variation of the voltage $V_c(t)$ but a variation of $I(t)$ containing somehow less noise than the Linsay case. In addition, the variation of $I(t)$ is similar to a relaxation oscillator with a noisy-slow episode followed by a sharp-fast episode.

Varactor.

In order to achieve their goal, they assumed that the diode will behave as an ideal diode with the following added characteristics:

1. There is a finite forward bias voltage V_f. The diode will not conduct until the forward voltage drop reaches V_f and the voltage drop remains at V_f as long as the diode conducts.

2. When the voltage drop is less than V_f, the diode does not conduct but acts as a capacitor with fixed capacitance.

3. When the current through the diode is driven through zero, the diode does not shut off immediately, but continues to conduct for a time equal to the reverse recovery time τ_{RR}.

While it is known that τ_{RR} depends on various factors such as the forward current and reverse voltage amplitudes, they chose a simple functional relationship to describe τ_{RR}:

$$\tau_{RR} = \tau_m(1 - \exp(-|I_m|/I_c)) \tag{19}$$

where $|I_m|$ is the most recent maximum forward current magnitude, and τ_m and I_c are parameters which describe the characteristics of the particular diode used.

In fact, charge storage time makes an important part of τ_{RR} and is given by:

$$\tau_S \approx \tau_{RR} \ln(1 + I_m/I_R) \tag{20}$$

where I_R is the reverse current through the diode during the storage phase.

This combined reverse-recovery-storage time approach allowed them to find an exact analytical solution to the Chaos transition problem.

In order to check Hunt [18] work, Mariz de Moraes and Anlage [20] explored Chaos transition in several RLD circuits while exploiting the properties of several types of diodes relating directly, resonance frequency f_0 to reverse recovery time τ_{RR}.

They found that when $f_0 \sim 100/\tau_{RR}$, Chaos transition disappears altogether (see Table 1).
This brings an additional deeper meaning to the appearance of Chaos:
"It is the coupling between the resonance frequency f_0 and $1/\tau_{RR}$ that brings about Chaos" and when they are uncoupled (in other words $f_0 \gg 1/\tau_{RR}$) Chaos is not possible. Another point of view of this argument came from the 1N4154 diode used by Linsay who had a very short τ_{RR} in the 2-4 ns range with a resonance frequency f_0 of 1.78 MHz leading us to the opposite limiting case: $f_0 \ll 1/\tau_{RR}$.

Combining both arguments, whether we have $f_0 \gg 1/\tau_{RR}$ or $f_0 \ll 1/\tau_{RR}$ no Chaos is expected since resonance and charge storage mechanisms are uncoupled whereas when $f_0 \sim 1/\tau_{RR}$ Chaos is possible since coupling between f_0 and τ_{RR} is optimally high.

Diode	τ_{RR} (ns)	C_0 (pF)	Results with $f_0 \sim 1/\tau_{RR}$	Results with $f_0 \sim 10/\tau_{RR}$	Results with $f_0 \sim 100/\tau_{RR}$
1N5400	7000	81	Period doubling and Chaos	Period doubling and Chaos	No period doubling nor Chaos
1N4007	700	19	Period doubling and Chaos	Period doubling and Chaos	No period doubling nor Chaos
1N5475B	160	82	Period doubling and Chaos	No period doubling nor Chaos	No period doubling nor Chaos
NTE610	45	16	Period doubling and Chaos	Period doubling under some conditions	No period doubling nor Chaos

Table 1: Period doubling and Chaos in driven RLD circuits with four different diodes. The reverse-recovery time τ_{RR} is given along with the zero-bias junction capacitance C_0. The resonant frequencies f_0 were changed by adjusting the L value in the RLD circuit, while R was fixed at 25 Ω. In comparison, the varactor diode 1N5470A used by Linsay [14] has C_0= 81.8 pF with τ_{RR} in the 100-200 ns, whereas Testa *et al.* [17] diode is 1N953 with C_0= 300 pF and τ_{RR} in the 100-200 ns as well. Adapted from Ref. [20].

Mariz de Moraes and Anlage [20] argument regarding Chaos transition in RLD circuits is that reverse recovery is indeed an essential effect producing Chaos in the sinusoidally driven RLD circuit.
However, both the reverse recovery and nonlinear capacitor models have memory built into them through a charge storage mechanism.

This led them to conclude that it is not useful to single out either the effect of nonlinear junction capacitance or reverse recovery time on minority carriers as the cause of Chaos, since both have similar effects on circuit dynamics. Moreover the reverse recovery time in real diodes is a strongly nonlinear function of forward-bias current, impacting frequency response, and dc bias.

III. COLPITTS OSCILLATOR

Now we move away from the RLD oscillator to replace the diode by a transistor and using two ordinary capacitors C_1 and C_2 with an inductance as a tuning resonator in order to describe the Colpitts circuit into its oscillatory or

chaotic modes, Thus, the Colpitts circuit, consists of a transistor providing amplification, in a feedback loop containing a parallel LC_1C_2 circuit operating as a bandpass filter to select the resonance frequency.
This is in fact a common-base Colpitts circuit, the voltage across C_2 being applied to the base-emitter junction of the transistor, as some feedback to stabilize oscillations.
In a common-collector version, the voltage across C_1 provides feedback. The frequency of oscillation is approximately the resonant frequency of the LC circuit, which is the series combination of C_1 and C_2 in parallel with the inductor:

$$f_0 = \frac{1}{2\pi\sqrt{L\frac{C_1C_2}{C_1+C_2}}} \tag{21}$$

The actual frequency of oscillation will be slightly lower due to junction capacitances and resistive loading of the transistor.

A. Simple Colpitts oscillator

Let us consider the circuit of fig. 14:

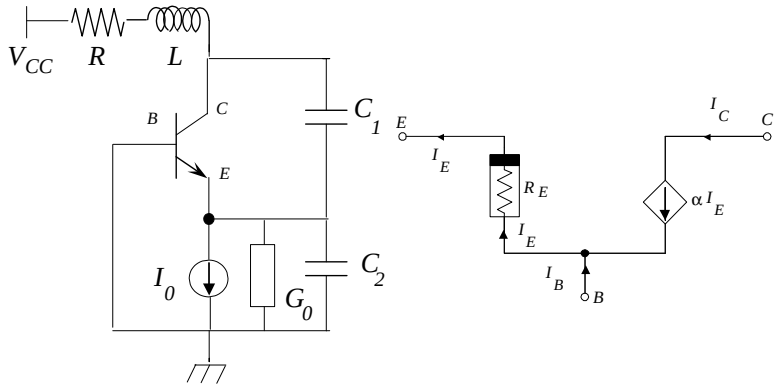

Fig.14: (left) Simple Colpitts oscillator and equivalent transistor circuit (right) with I_0 the constant current source, I_S the transistor saturation current and R_E the emitter variable resistor.

The state-space equations for the circuit are:

$$\begin{aligned} C_1\frac{dV_{C_1}}{dt} &= -\alpha f_E(-V_{C_2}) + I_L \\ C_2\frac{dV_{C_2}}{dt} &= (1-\alpha) f_E(-V_{C_2}) + I_L - I_0 \\ L\frac{dI_L}{dt} &= -V_{C_1} - V_{C_2} - RI_L + V_{CC} \end{aligned} \tag{22}$$

where f_E is the driving-point characteristic of the emitter non-linear resistor of the transistor. It can be expressed in the form $I_E = f_E(V_{BE}) = f_E(-V_{C_2})$ which may be represented mathematically by a piece-wise linear system for the transistor emitter current:

$$I_E = I_0\frac{V_{BE}-V_{th}}{V_T}, \quad V_{BE} \geq V_{th} \text{ (forward active case)}, \quad I_E = 0, \quad V_{BE} < V_{th} \text{ (cut-off case)} \tag{23}$$

where V_{th} is the threshold voltage: $V_{th} = k_BT[\ln(\alpha I_S/I_0) - 1]$ and I_S the saturation current.
This originates from the fact, the emitter current is given by: $I_E = I_s\left[e^{\frac{V_{BE}}{k_BT}} - 1\right]$ resulting into $f_E(V_C) = I_s e^{-\frac{V_C}{k_BT}}$ when $V_C \gg k_BT$.

Kennedy [21] *et al.* evaluated the phase diagram in terms of two parameters g^*, Q where g^* is the open loop gain such that the Barkhausen condition id $g^* = 1$ and the quality factor $Q = L\omega/R$ where $\omega = 2\pi f_0$. They found that oscillatory behavior implies $g^* < 1$ whereas chaotic behavior implies $g^* > 10$.

In order to find the detailed time dependence of system 22 we use order-4 Runge-Kutta method of integration [16]. Oscillatory behavior with $f_0 = 97.84$ kHz is displayed in fig. 15.

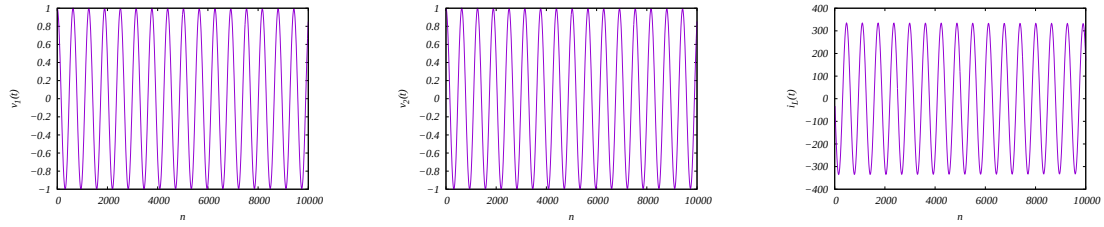

Fig.15: Oscillatory response of the Colpitts circuit. The voltages $v_1(t), v_2(t)$ are across the corresponding capacitors and $i_L(t)$ is the current intensity across the inductor. $C_1 = 54.$nF, $C_2 = 54.$ nF and $L = 98.\mu$H, $R = 0.1\Omega$ and g^* =0.9

B. Chaotic Colpitts oscillator

Driving the Colpitts oscillator into a chaotic regime entails using different circuit parameters and initial conditions.

Chaotic response is displayed below in fig. 16:

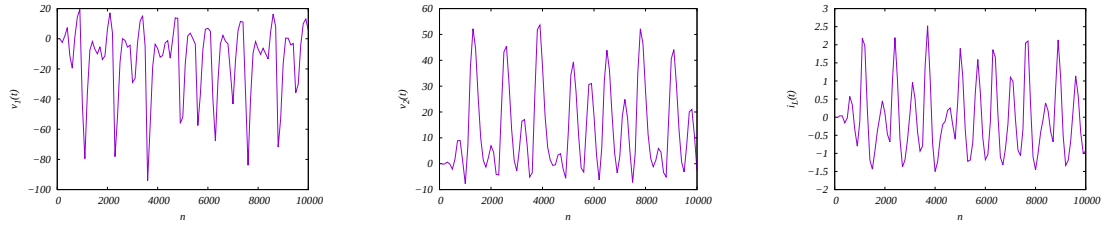

Fig.16: Chaotic response of the Colpitts circuit. The voltages $v_1(t), v_2(t)$ are across the corresponding capacitors and $i_L(t)$ is the current intensity across the inductor. $C_1 = 54.$nF, $C_2 = 54.$ nF and $L = 98.\mu$H, $R = 40\Omega$ and $g^* = 20.$

APPENDIX A: Saddle-Node Bifurcation

Saddle-node bifurcation occurs when fixed points are created or destroyed by changes of a control parameter. A simple example of a saddle-node bifurcation is given by the first-order system:
$\dot{x} = r + x^2$ where r is a parameter. When r is negative, there are two fixed points given by $\dot{x} = 0$, or $r + x^2 = 0$ whose solutions are $x_{1,2} = \pm\sqrt{-r}$ implying that r should be negative for real valued fixed points as displayed in fig. 17.

When $r < 0$ the parabola $r + x^2$ cuts the x axis at two fixed points $x_{1,2} = \pm\sqrt{-r}$ that coalesce into a single fixed point at $x^* = 0$ when $r = 0$. Finally when $r > 0$, there are no fixed points since $x_{1,2} = \pm\sqrt{-r}$ become imaginary.

In order to tackle stability, there are two cases to consider:
1- Discrete time or map function case: $x_{n+1} = f(x_n)$ where x, f are real scalars or vectors.

2- Continuous time or ODE system case: $\dot{x} = f(x)$ where x, f are real scalars or vectors.

Stability analysis is obtained from exploring the neighborhood of the fixed point $x^* = f(x^*)$ in the discrete case or $\dot{x}_{x=x^*} = 0$ in the continuous case.
In the map case, $x_{n+1} = f(x_n)$, should be expanded around the fixed point $x^* = f(x^*)$. This yields $x^* + \epsilon_{n+1} = f(x^* + \epsilon_n) \approx f(x^*) + \epsilon_n(\frac{df}{dx})_{x^*}$. Thus $\epsilon_{n+1} = a\epsilon_n$ with $a = (\frac{df}{dx})_{x^*}$ the amplification factor. We deduce that the fixed point is attractive (stable) if $|a| \leq 1$ and repulsive (unstable) if $|a| > 1$.

In the ODE system case $\dot{\boldsymbol{x}} = \boldsymbol{f}(\boldsymbol{x})$, we linearize the system, evaluate the Jacobian matrix given that in the general case $\boldsymbol{x} = (x_1, x_2, ...)$:

$$\frac{\partial(\dot{x_1}, \dot{x_2}, \dot{x_3}...)}{\partial(x_1, x_2, x_3...)} \tag{A1}$$

and extract its eigenvalues whose signs at the respective fixed points determine stability.

In the discrete map case $\boldsymbol{x}_{n+1} = \boldsymbol{f}(\boldsymbol{x}_n)$, $\boldsymbol{x} = (x_1, x_2, ...), \boldsymbol{f} = (f_1, f_2, ...)$ we linearize the map to evaluate the Jacobian matrix elements J_{ij} as:

$$J_{ij} = \left(\frac{\partial f_i}{\partial x_j}\right) \tag{A2}$$

and extract its eigenvalues whose signs at the respective fixed points determine stability.

Applying the above to $r < 0$ we obtain $\lambda_{1,2} = 2x_{1,2}$ with $x_{1,2} = \pm\sqrt{-r}$, thus $\lambda_1 = -\sqrt{-r}$ negative, consequently x_1 is stable whereas $\lambda_2 = \sqrt{-r}$ is positive implying x_2 is unstable.

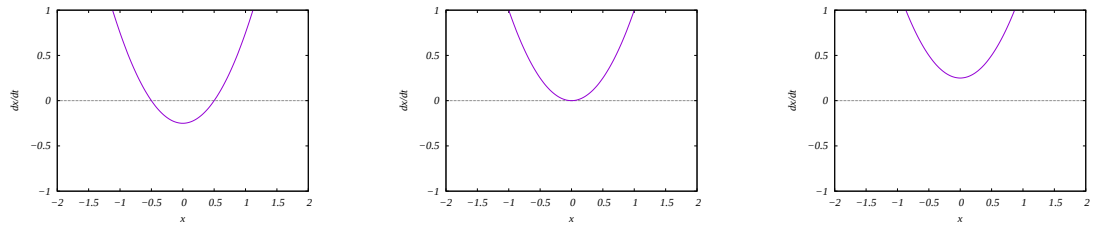

Fig.17: Saddle-node bifurcation viewed in the phase plane $\dot{x}, x$ for the system $\dot{x} = r + x^2$. When $r < 0$ there are two fixed points $x^* = \pm\sqrt{-r}$ collapsing into a single point $x^* = 0$ when $r = 0$, to finally absence of fixed points when $r > 0$.

Note: A straightforward criterion to tell whether a 1D function map $f(x)$ is chaotic or not is given by a negative sign of the Schwarzian derivative [1]:

$$Sf(x) = \frac{f'''}{f'} - \frac{3}{2}\left(\frac{f''}{f'}\right)^2, \quad f' = \frac{df}{dx}, f'' = \frac{d^2f}{dx^2}, f''' = \frac{d^3f}{dx^3} \tag{A3}$$

For instance in the case of the logistic map, $Sf(x)$ is negative over the entire interval $[0, 1]$.

APPENDIX B: Hopf bifurcation

Hopf bifurcation occurs when a stable fixed point becomes unstable under the action of a control parameter μ. Let us start from some two-dimensional system with a fixed point. If the fixed point is stable, the eigenvalues λ_1, λ_2 must both lie in the left half-plane $Re\lambda < 0$.
Since the λ's satisfy a quadratic equation with real coefficients, there are two possible cases: either the eigenvalues are both real and negative or they are complex conjugates. In order to destabilize the fixed point, we need one or both of the eigenvalues to cross into the right half-plane $Re\lambda > 0$ as μ varies.

1. Supercritical Hopf Bifurcation

Consider a physical system that settles down to equilibrium with exponentially damped oscillations. If we suppose the decay rate depends on a control parameter μ, it becomes slower and slower and finally changes to growth at a critical value μ_c where the equilibrium state will lose stability. In many cases the resulting motion is a small-amplitude, sinusoidal, limit cycle or closed orbit oscillation about the former steady state. Then the system is considered to have experienced a supercritical Hopf bifurcation.

A supercritical Hopf bifurcation occurs when a stable spiral, in phase space, changes into an unstable spiral surrounded by a small, nearly elliptical limit cycle. Hopf bifurcations can occur in phase spaces of any dimension $n \neq 2$, nonetheless, we restrict ourselves to two dimensions.

A simple example of a supercritical Hopf bifurcation is given by the following continuous time first-order ODE 2D system [9]:

$$\begin{aligned} \dot{r} &= \mu r - r^3, \\ \dot{\theta} &= \omega + br^2 \end{aligned} \tag{B1}$$

There are three parameters: μ controls the stability of the fixed point at the origin, ω gives the frequency of infinitesimal oscillations, and b determines the dependence of frequency on amplitude for larger amplitude oscillations.

When $\mu < 0$, the origin $r = 0$ is a stable spiral whose sense of rotation depends on the sign of ω. For $\mu = 0$ the origin is a stable spiral. When $\mu > 0$ there is an unstable spiral at the origin and a stable circular limit cycle at $r = \sqrt{\mu}$.

2. Subcritical Hopf Bifurcation

Type II intermittency and Lorenz system behavior are due to a subcritical Hopf bifurcation. Following the supercritical case, an example of a subcritical Hopf bifurcation is given by the following continuous time first-order ODE 2D system [9]:

$$\begin{aligned} \dot{r} &= \mu r + r^3 - r^5, \\ \dot{\theta} &= \omega + br^2 \end{aligned} \tag{B2}$$

The difference between the previous system by eqs. (B1) and the current given by eqs. (B2) is that the cubic term r^3 now drives the phase-space trajectories away from the origin unlike the supercritical case.

3. Degenerate Hopf Bifurcation

An example is given by the damped pendulum

$$J\ddot{\theta} = F\ell\cos(\omega t) - mg\ell\sin(\theta) - \gamma\ell\dot{\theta} \tag{B3}$$

As we change the damping γ from positive to negative, the fixed point at the origin changes from a stable to an unstable spiral. However at $\gamma = 0$ we do not have a true Hopf bifurcation because there are no limit cycles on either side of the bifurcation.

This case typically arises when a non-conservative system suddenly becomes conservative at the bifurcation point. The fixed point becomes a nonlinear center, rather than the weak spiral required by a Hopf bifurcation.

4. Hopf bifurcation and the Lorenz system

The Rayleigh-Bénard experiment mimics interaction between the Sun and an approximately flat Earth atmosphere in order to understand weather and model climate. Coupling of the Navier-Stokes equations with thermal convection,

it is a 2D problem describing thermal convection between two parallel horizontal plates at different temperatures sandwiching a fluid representing the atmosphere.
The Lorenz system is derived from a modal expansion of the Oberbeck-Boussinesq approximation with an additional truncation of the Fourier-Galerkin expansion [22].
The system is obtained as:

$$\begin{aligned} \dot{x} &= \sigma(y-x) \\ \dot{y} &= \rho x - y - xz \\ \dot{z} &= xy - \beta z \end{aligned} \tag{B4}$$

with $\sigma, \beta, \rho \geq 0$. σ corresponds to Prandtl number, β is a geometric parameter and ρ is the Rayleigh number in units of the critical Rayleigh number [22].

These equations describe a dissipative dynamical system for all values of ρ, σ and β because the divergence of the flow field (or the ODE system) is always negative [22].

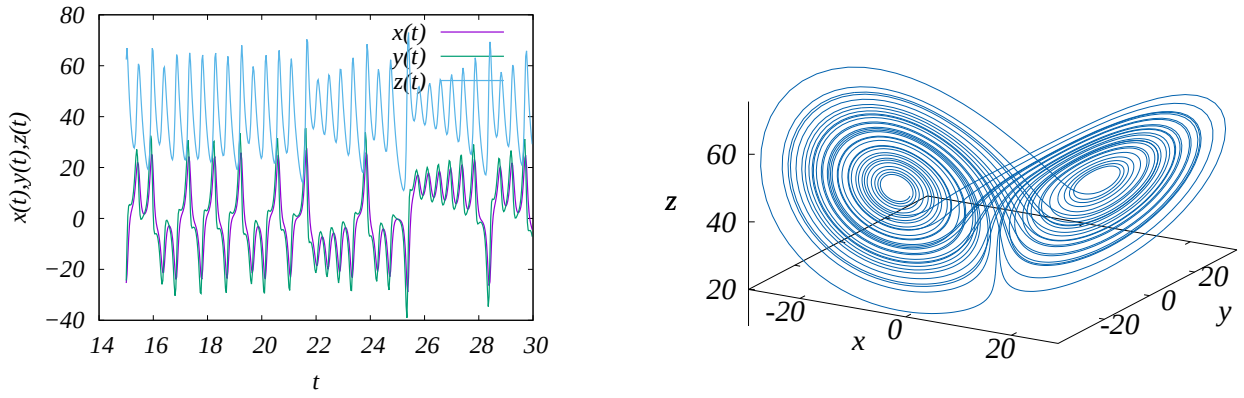

Fig.18: (Left) $x(t), y(t), z(t)$ time series with parameters $\sigma = 16, \beta = 4, \rho = 45.92$ and timestep equal to 0.03. (Right) 3D Lorenz butterfly attractor using a timestep equal to 0.005 for orbit smoothness.

The eigenvalues are evaluated as usual, by linearizing the system B4 to obtain the Jacobian matrix

$$\frac{\partial(\dot{x}, \dot{y}, \dot{z})}{\partial(x, y, z)} = \begin{pmatrix} -\sigma & \sigma & 0 \\ -\rho - z & -1 & -x \\ y & x & -\beta \end{pmatrix} \tag{B5}$$

whose characteristic polynomial is:
$P(\lambda) = -\lambda^3 - (\beta + \sigma + 1)\lambda^2 - \frac{1}{2}(2\sigma(\rho - z) - 2x^2 + \beta^2 + 1 + \sigma^2) - (\beta + \sigma + 1)^2)\lambda + \rho\beta(\sigma - z - 1) - \sigma x(x + y)$
We infer that when $0 < \rho < 1$, only one stable fixed point exists $x^* = y^* = z^* = 0$,
However when $\rho > 1$ we get three fixed points:

$$x^* = y^* = \pm\sqrt{\beta(\rho - 1)}\ ,\ z^* = \rho - 1, \tag{B6}$$

For $\rho > 1$, fixed point $x^* = y^* = z^* = 0$ is unstable, whereas fixed points given by eq. B6 are stable if $0 < \sigma < \beta + 1$. However, if $\sigma > \beta + 1$, fixed points B6 are unstable when $\rho > \sigma(\sigma + \beta + 3)/(\sigma - \beta - 1)$ and a strange attractor as in fig.18 appears.

A pitchfork bifurcation occurs at $\rho = 1$, and if $\sigma > \beta + 1$, a subcritical Hopf bifurcation occurs at $\rho = \sigma(\sigma + \beta + 3)/(\sigma - \beta - 1)$.

It can be proven that $\sigma(\sigma + \beta + 3)/(\sigma - \beta - 1) > 1$ for any available β when $\sigma > \beta + 1$.

The attractor is the set of points in phase space that can be arrived at when time $t \to +\infty$ starting from some arbitrary initial condition at $t = 0$.

The two fundamental properties of strange attractors are:

- it is invariant under the evolution.
- the distance of any solution from it vanishes as $t \to +\infty$.
- They possess a fractal self-similar geometry.

The second property simply means that if the solution is initially outside the attractor, it will reach it when $t \to +\infty$ and stays on it once inside.

References

[1] H. G. Schuster and W. Just, *Deterministic Chaos: An Introduction*, Fourth Edition, Wiley-VCH (2005).

[2] L. D. Landau and E. M. Lifshitz, *Fluid Mechanics*, First edition MIR, Moscow (1971) and Second edition, Pergamon, Oxford (1987).

[3] S. Newhouse, D. Ruelle and F. Takens, Commun. Math. Phys. **64**, 35 (1978)

[4] T. S. Parker and L. O. Chua, *Practical numerical algorithms for chaotic systems*, Springer-Verlag, New York, First edition (1989).

[5] M. J. Feigenbaum, J. Stat. Phys. 19, 25 (1978), J. Stat. Phys. 21, 666 (1979) and Commun. Math. Phys. 77, 65 (1980).

[6] H. O. Peitgen and P. H. Richter, *The Beauty of Fractals*, Springer, Berlin-Heidelberg (1986).

[7] A. B. Carlson and P. B. Crilly *Communication systems: An Introduction to Signals and Noise in Electrical Communication*, 5th Edition, McGraw-Hill, New York (2010).

[8] Y. Pomeau, and P. Manneville, *Intermittent transition to turbulence in dissipative dynamical systems*. Communications in Mathematical Physics 74 189-97 (1980).

[9] S. H. Strogatz, *Nonlinear dynamics and Chaos: with applications to physics, biology, chemistry, and engineering*, Perseus Books Publishing, L.L.C. 1994

[10] K. Ikeda and O. Akimoto, Phys. Rev. Lett. **48**, 617 (1982). See also: P. Mandel, R. Kapral, *Subharmonic and chaotic bifurcation structure in optical bistability*, Opt. Comm. **47**, 151 (1983).

[11] S. M. Hammel, C. K. R. T. Jones and J. V. Moloney, J. Opt. Soc. Am. **B4**, 552 (1985), see also: J. V. Moloney, Opt. Comm. **48**, 435 (1984).

[12] P. Nardone, P. Mandel, R. Kapral, *Analysis of a delay-differential equation in optical bistability*, Phys. Rev. A **33**, 2465 (1986).

[13] C. Grebogi, E. Ott, E., and J. A. Yorke, *Are Three-Frequency Quasi-Periodic Orbits to be Expected in Typical Nonlinear Systems?*, Phys. Rev. Lett. **51**, 339. (1983)

[14] P. S. Linsay, *Period Doubling and Chaotic Behavior in a Driven Anharmonic Oscillator*, Phys. Rev. Lett. 47, 1349 (1981).

[15] I. Kovacic and M. J. Brennan, *The Duffing Equation: Nonlinear Oscillators and their behavior*, Wiley (2011).

[16] W. H. Press, W. T. Vetterling, S. A. Teukolsky and B. P. Flannery, *Numerical Recipes in C: The Art of Scientific Computing* Third Edition, Cambridge University Press, New-York (2007).

[17] J. Testa, J. Perez, and C. Jeffries, *Evidence for Universal Chaotic Behavior of a Driven Nonlinear Oscillator*, Phys. Rev. Lett. **48**, 714 (1982).

[18] E. R. Hunt, Phys. Rev. Lett. 49, 1054 (1982) and R. W. Rollins and E. R. Hunt *Exactly Solvable Model of a Physical System Exhibiting Universal Chaotic Behavior* Phys. Rev. Lett. 49, 1295 (1982).

[19] P. Horowitz and W. Hill, *The Art of Electronics*, Third Edition, Cambridge University Press (2015). See also S. M. Sze,*Physics of semiconductor devices* Second Edition, Wiley-Interscience (1981) and G. Neudeck, *The PN junction diode*, Second Edition, Volume 2, Addison-Wesley Modular Series on Solid State Devices (1989).

[20] R. Mariz de Moraes and S. M. Anlage, *Unified model and reverse recovery nonlinearities of the driven diode resonator*, Phys. Rev. E **68**, 026201 (2003).

[21] G. M Maggio, O. De Feo, and M. P. Kennedy, IEEE Trans. on Circuits and Systems I: *Fundamental Theory and Applications*, **46**, 1118 (1999).

[22] Sparrow C., *The Lorenz Equations: Bifurcations, Chaos and Strange Attractors*, Springer Series in Applied Mathematics **41**, Springer-Verlag (1982)